High-spin excitations in ^{158,159,160}Hf from recoil-decay tagging

K. Y. Ding,[1,*] J. A. Cizewski,[1] D. Seweryniak,[2] H. Amro,[2,†] M. P. Carpenter,[2] C. N. Davids,[2] N. Fotiades,[1,‡] R. V. F. Janssens,[2] T. Lauritsen,[2] C. J. Lister,[2] D. Nisius,[2,§] P. Reiter,[2,‖] J. Uusitalo,[2,¶] I. Wiedenhöver,[2] and A. O. Macchiavelli[3]

[1]*Department of Physics and Astronomy, Rutgers University, New Brunswick, New Jersey 08903*

[2]*Argonne National Laboratory, Argonne, Illinois 60439*

[3]*Nuclear Science Division, Lawrence Berkeley National Laboratory, Berkeley, California 94720*

(Received 18 May 2000; published 21 August 2000)

The 270-MeV ^{58}Ni+^{A}Pd reaction was used for the first recoil-decay tagging measurement with Gammasphere coupled to the Fragment Mass Analyzer at Argonne National Laboratory. Level structures of ^{158}Hf and ^{159}Hf are identified for the first time, and that of ^{160}Hf is extended. The systematical behavior of the energy levels in neighboring isotones and isotopes, as well as the aligned angular momenta as a function of rotational frequency, are examined.

PACS number(s): 27.70.+q, 23.20.Lv, 23.20.En

I. INTRODUCTION

Nuclei above the ^{146}Gd core with $N \geqslant 82$ and $Z \geqslant 64$ exhibit a wide variety of shapes. For nuclei with $82 \leqslant N \leqslant 84$, the level structures can be understood as resulting from the interactions of a few valence nucleons outside the closed shells, and angular momentum is generated by the alignment of the spins of individual nucleons, e.g., Refs. [1,2]. Nuclei with $N \geqslant 90$ are prolate deformed and the level structures are characterized by rotational bands built upon the deformed configurations, e.g., Refs. [3,4]. In transitional nuclei, with $86 \leqslant N < 90$, both rotational and single-particle degrees of freedom can coexist and generate angular momentum in the same nucleus. At high spins, band termination, which occurs when the spins of all of the valence nucleons are aligned, has been previously observed in the $N = 88,90$, $Z \geqslant 64$ isotones, e.g., Refs. [5–7].

The present work studies the structural changes induced by the increase in angular momentum, as well as by the change in proton and neutron numbers, in the transitional nuclei $^{158-160}$Hf. The nuclei ^{158}Hf and ^{159}Hf are the most proton-rich $N = 86$ and $N = 87$ isotones in which excited states have been studied thus far.

II. EXPERIMENT

The ^{A}Pd(^{58}Ni, $xpynz\alpha$) reactions with a beam energy of 270 MeV were used to populate the high-spin states in $^{158-160}$Hf. The target, chosen to study the excited states in the proton-rich $N = 84$ isotones above the ^{146}Gd core, was 1-mg/cm^2 thick and consisted of ^{102}Pd (69%), ^{104}Pd (12%), ^{105}Pd (6%), and ^{106}Pd (6%). The experiment was the first Gammasphere (GS) measurement using the recoil-decay tagging (RDT) technique at Argonne National Laboratory. These reactions have a large number of particle-evaporation channels, and an additional complication comes from the relatively low enrichment of the target. Data on ^{158}Hf, ^{159}Hf, and ^{160}Hf are discussed in this work; results on ^{155}Yb, ^{155}Lu, ^{156}Lu, and ^{157}Lu will be presented elsewhere [8].

The projectile, ^{58}Ni, was accelerated by the Argonne Tandem Linear Accelerator System (ATLAS). The GS array consisted of 101 Compton-suppressed Ge detectors. The Fragment Mass Analyzer (FMA) [9], located downstream from GS, was used to disperse the evaporation residues according to their mass-to-charge (M/Q) ratio, and to suppress the contributions from fission and scattered beam. The positions of the recoils at the focal plane of the FMA were determined by using a position-sensitive Parallel-Grid Avalanche Counter (PGAC). The recoils were subsequently implanted in a 48×48, 60-μm thick double-sided silicon-strip detector (DSSD) placed 40 cm behind the PGAC.

The data from the experiment were recorded by the GS acquisition system and written to magnetic tapes for off-line analysis. The GS pretrigger condition required at least two Ge detectors to fire. In addition, there was an external pretrigger in the GS data acquisition for this experiment. The main trigger of an event required signals from at least two Compton-suppressed Ge detectors and the PGAC, or any event in which the DSSD recorded a recoil or decay event. The information recorded on magnetic tape for subsequent analysis included γ-ray energies (E_γ) and times with respect to the radio frequency (RF) of the accelerator, the position (X_{PGAC} and Y_{PGAC}) and energy loss (ΔE_r) of the evaporation residues in the PGAC, and the strip numbers (X,Y) and energy (E_r) of recoils in the DSSD, as well as the energy (E_α) and strip numbers (X,Y) of the decay particles associated with the implanted residues. The time of flight (TOF) of the recoils between (i) the PGAC and DSSD and (ii) the

*Present address: Telcordia Technologies, Piscataway, NJ 08854.

†Present address: Mississippi State University, Mississippi St., MS 39762.

‡Present address: Los Alamos National Laboratory, Los Alamos, NM 87545.

§Present address: Bio-Imaging Research, Lincolnshire, IL 60069.

‖Present address: Ludwig Maximilian Universität München, Garching, Germany.

¶Present address: University of Jyväskylä, 40351 Jyväskylä, Finland.

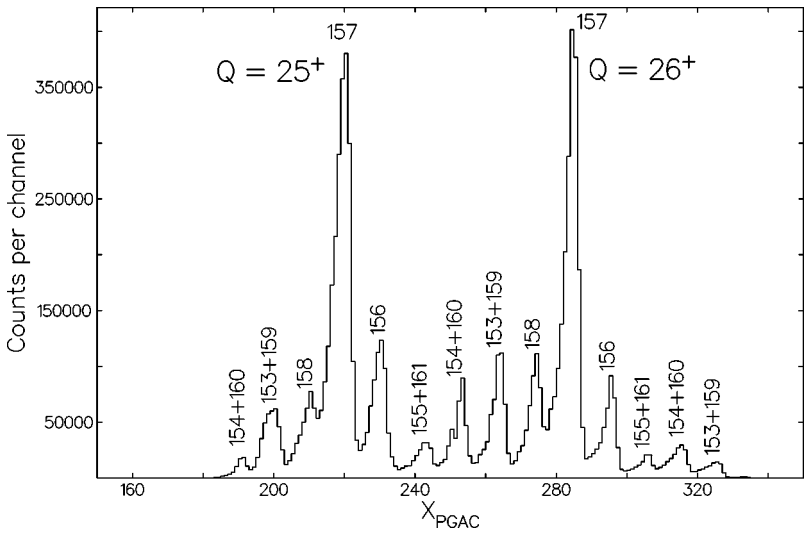

FIG. 1. Projection of the X_{PGAC} vs E_γ matrix onto the X_{PGAC} axis. Masses of the recoils are labeled, as well as the 25^+ and 26^+ charge states of the dominant $A=157$ channels.

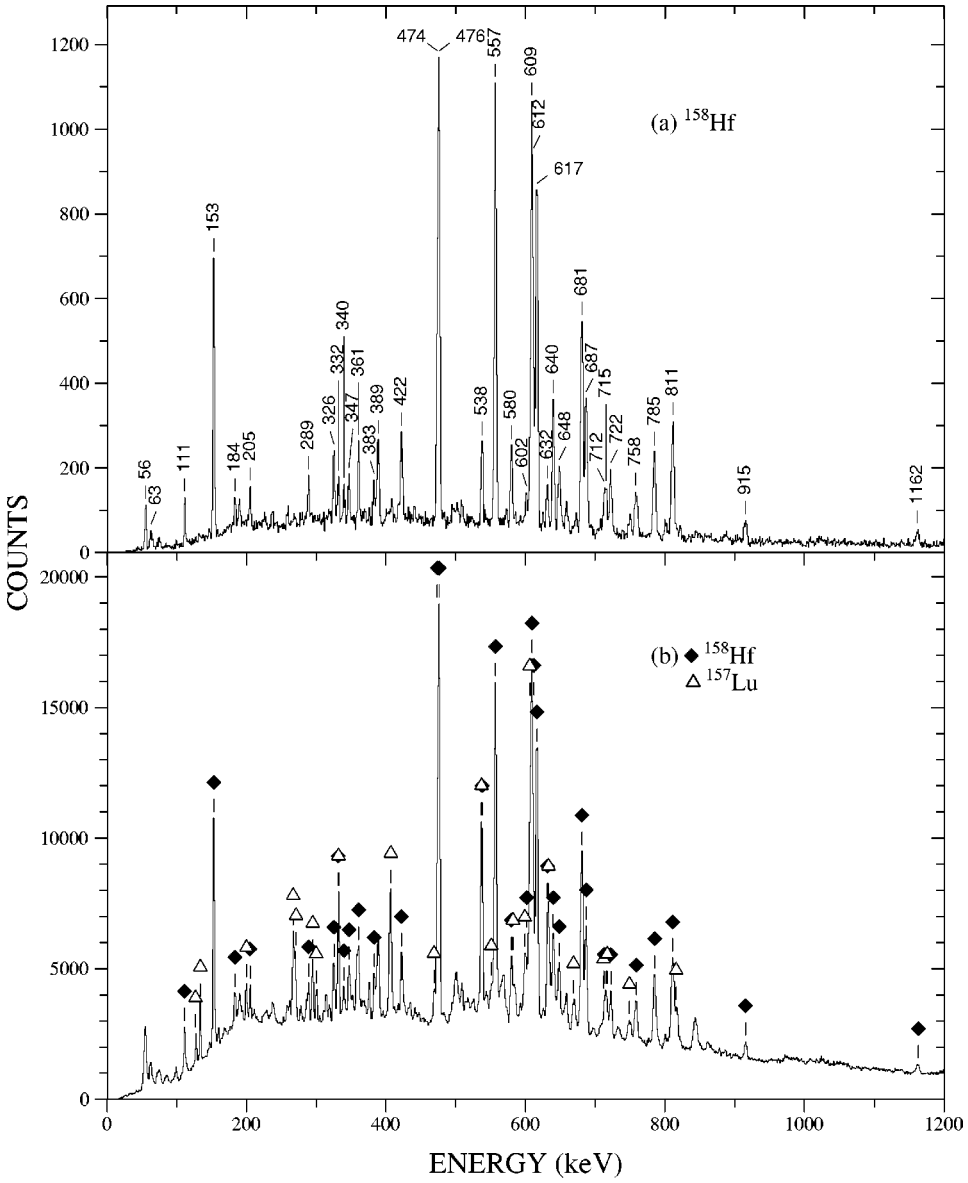

FIG. 2. (a) Total projection of the γ-ray events gated on $A=158$ and the α decay of ^{158}Hf ($E_\alpha=5.269$ MeV, $t_{1/2}=2850$ ms). (b) Total projection of the γ-ray events gated on $A=158$.

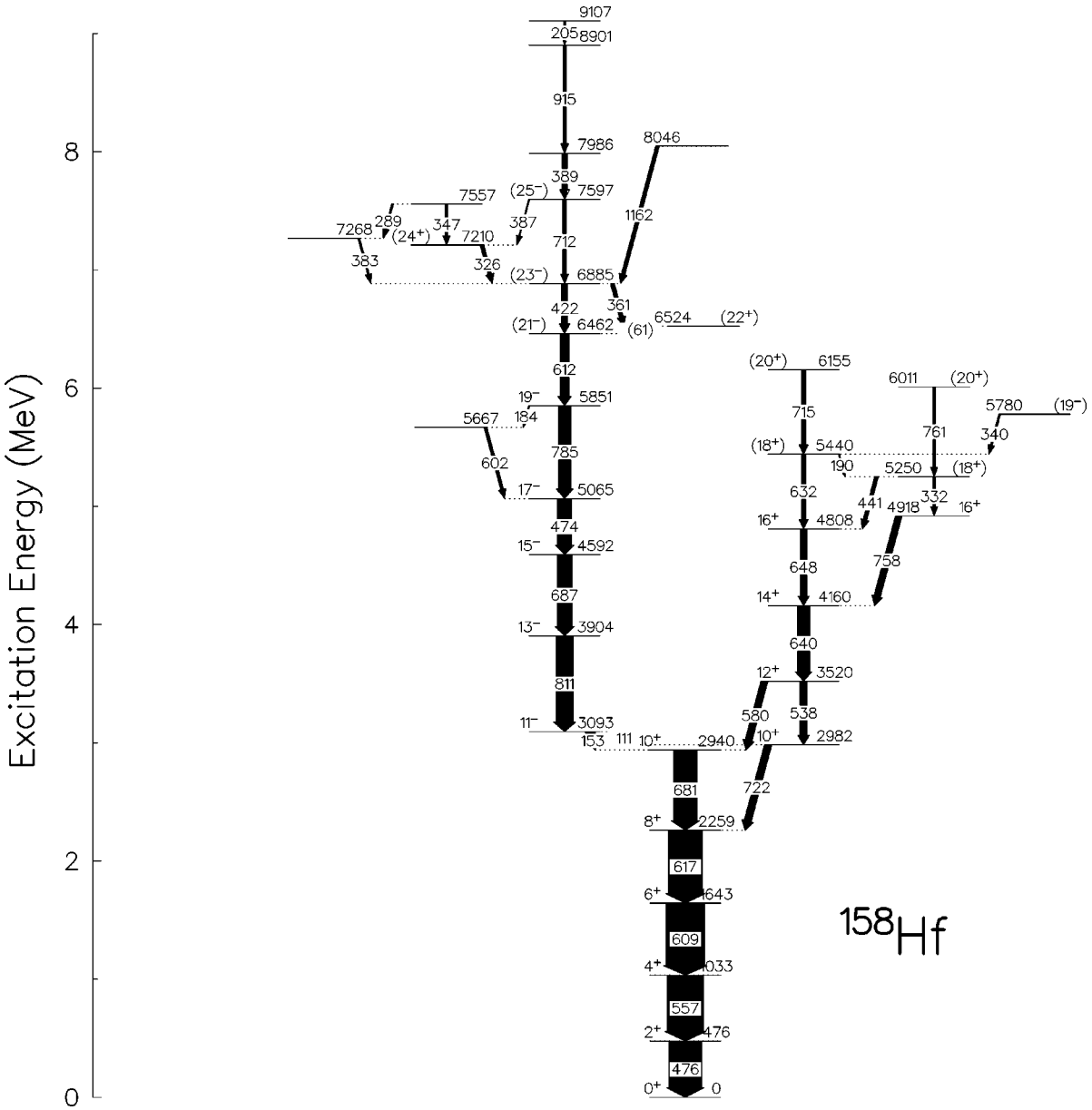

FIG. 3. Level scheme of ^{158}Hf. The widths of the arrows are proportional to the γ-ray intensities.

prompt γ-ray flash at the target position and the PGAC were also recorded. In addition, the time from an absolute clock was recorded for every event throughout the experiment to determine the time elapsed between implantation and decay of a recoil. The correlations between prompt γ rays and particle-decay events in the DSSD were established in the off-line analysis.

Standard γ-ray sources of ^{152}Eu, ^{182}Ta, ^{56}Co, and ^{243}Am were used for energy and efficiency calibrations of the Ge detectors.

The FMA was tuned so that both 25^+ and 26^+ charge states of $A\sim157$ recoils could be collected at the focal plane. The prompt recoil-γ coincidence events were sorted into a X_{PGAC} vs E_γ matrix. The projection of this matrix onto the X_{PGAC} axis is shown in Fig. 1. The nuclei of masses from 158 to 161 were probably produced by the fusion of the beam and the heavier Pd contaminants in the target. The M/Q ratio positions of the $A=159-161$ isobars overlapped the focal plane positions of the $A=153-155$ isobars with the neighboring charge states. By gating on the X_{PGAC} of a particular nucleus and on the corresponding E_α energy and lifetime of an isomer in the nucleus, a γ-γ matrix for a specific isomer could be constructed and the γ-ray transitions associated with that channel could be studied. Angular distributions of the γ-ray intensities were used to deduce the multipolarities of transitions, since the statistics were not sufficient for directional correlation analyses. Further details of the experiment and analysis are presented in Ref. [10].

III. ANALYSIS AND RESULTS

A. Level scheme of ^{158}Hf

^{158}Hf was produced by either the fusion of the beam and the ^{102}Pd target or the beam and the $^{104-106}$Pd contaminants

TABLE I. Energies, relative intensities, a_2 coefficients, and placements of γ-ray transitions in ^{158}Hf. Spin-parities in parentheses are tentatively established.

Energy (keV)	Intensity	a_2	Mult.	E_x (keV)		Assignment		
				E_i	E_f	I_i^π	→	I_f^π
61.3(3)	27(7)		$E1$	6524	6462	(22^+)	→	(21^-)
111.49(12)	45(6)	−0.76(14)	$E1$	3093	2981	11^-	→	10^+
153.14(10)	235(20)	−0.50(5)	$E1$	3093	2940	11^-	→	10^+
183.6(2)	29(7)			5851	5667			
189.9(2)	23(6)			5440	5250	(18^+)	→	(18^+)
205.31(14)	44(8)			9107	8901			
289.07(15)	51(8)	0.42(11)	$E2$	7557	7268			
325.64(12)	95(12)	−0.30(11)	$E1$	7210	6885	(24^+)	→	(23^-)
331.70(14)	64(9)		$(E2)$	5250	4918	(18^+)	→	16^+
339.9(2)	46(8)	−0.41(29)	$E1$	5780	5440	(19^-)	→	(18^+)
346.97(14)	66(9)			7557	7210	(26^+)	→	(24^+)
360.94(12)	112(13)	−0.42(17)	$(E1)$	6885	6521	(23^-)	→	(22^+)
383.3(2)	51(9)			7268	6885			
386.8(5)	<29			7597	7210	(25^-)	→	(24^+)
388.72(12)	143(14)			7986	7596			
422.37(12)	160(15)	0.30(10)	$E2$	6885	6462	(23^-)	→	(21^-)
441.3(4)	24(9)		$(E2)$	5250	4808	(18^+)	→	16^+
473.95(11)	387(46)	0.15(11)	$E2$	5065	4592	17^-	→	15^-
476.36(11)	887(60)	0.22(6)	$E2$	476	0	2^+	→	0^+
537.95(12)	193(16)		$E2$	3520	2928	12^+	→	10^+
556.97(10)	≡1000		$E2$	1033	476	4^+	→	2^+
579.89(13)	189(16)	0.24(16)	$E2$	3520	2940	12^+	→	10^+
601.6(2)	83(11)			5667	5065			
609.28(11)	1074(76)	0.16(9)	$E2$	1643	1033	6^+	→	4^+
611.7(4)	245(56)		$(E2)$	6462	5851	(21^-)	→	19^-
616.63(11)	962(49)	0.11(5)	$E2$	2259	1643	8^+	→	6^+
631.7(2)	117(12)		$(E2)$	5440	4808	(18^+)	→	(16^+)
639.79(12)	326(22)	0.29(6)	$E2$	4160	3520	14^+	→	12^+
648.36(14)	179(15)	0.42(7)	$E2$	4808	4160	16^+	→	14^+
680.89(10)	650(36)	0.32(6)	$E2$	2940	2259	10^+	→	8^+
687.09(11)	424(27)	0.44(7)	$E2$	4592	3904	15^-	→	13^-
712.5(5)	92(21)		$(E2)$	7597	6885	(25^-)	→	(23^-)
715.4(3)	121(22)		$(E2)$	6155	5440	(20^+)	→	(18^+)
722.31(14)	200(17)	0.40(7)	$E2$	2982	2259	10^+	→	8^+
758.2(3)	177(16)	0.32(14)	$E2$	4918	4160	16^+	→	14^+
761.2(8)	58(30)		$(E2)$	6011	5250	(20^+)	→	(18^+)
785.17(12)	341(24)	0.23(8)	$E2$	5851	5065	19^-	→	17^-
811.18(13)	478(31)	0.24(5)	$E2$	3904	3093	13^-	→	11^-
915.4(2)	79(10)	0.36(10)	$E2$	8901	7986			
1161.7(3)	76(14)			8046	6885			

in the target. The total projection of the γ-ray events gated on $A=158$ and on the α decay of ^{158}Hf ($E_\alpha=5.269$ MeV and $t_{1/2}=2850$ ms) [11] is shown in Fig. 2(a). The total projection of the γ-ray events gated on $A=158$ alone is displayed in Fig. 2(b). Transitions from ^{157}Lu are also observed in this spectrum because of the contamination of the $A=158$ mass peak by the tail of the strong $A=157$ channels. Given that many of the transitions which are strong in Fig. 2(a) are also strong in Fig. 2(b), a γ-γ matrix gated on $A=158$ with enhanced statistics was used to determine the level scheme of ^{158}Hf. Nevertheless, the spectrum in Fig. 2(a) provides a unique identification of the transitions which belong to ^{158}Hf.

The extensive level scheme of ^{158}Hf up to $E_x \sim 9.1$ MeV and $I \gtrsim 25\hbar$, shown in Fig. 3, is based on coincidence relationships and relative intensities. The summary of the γ-ray transitions in ^{158}Hf is displayed in Table I. The relative intensities were obtained from the total projection gated on $A=158$ and the α decay of ^{158}Hf. Although transitions have been previously observed in ^{158}Hf [12], the level

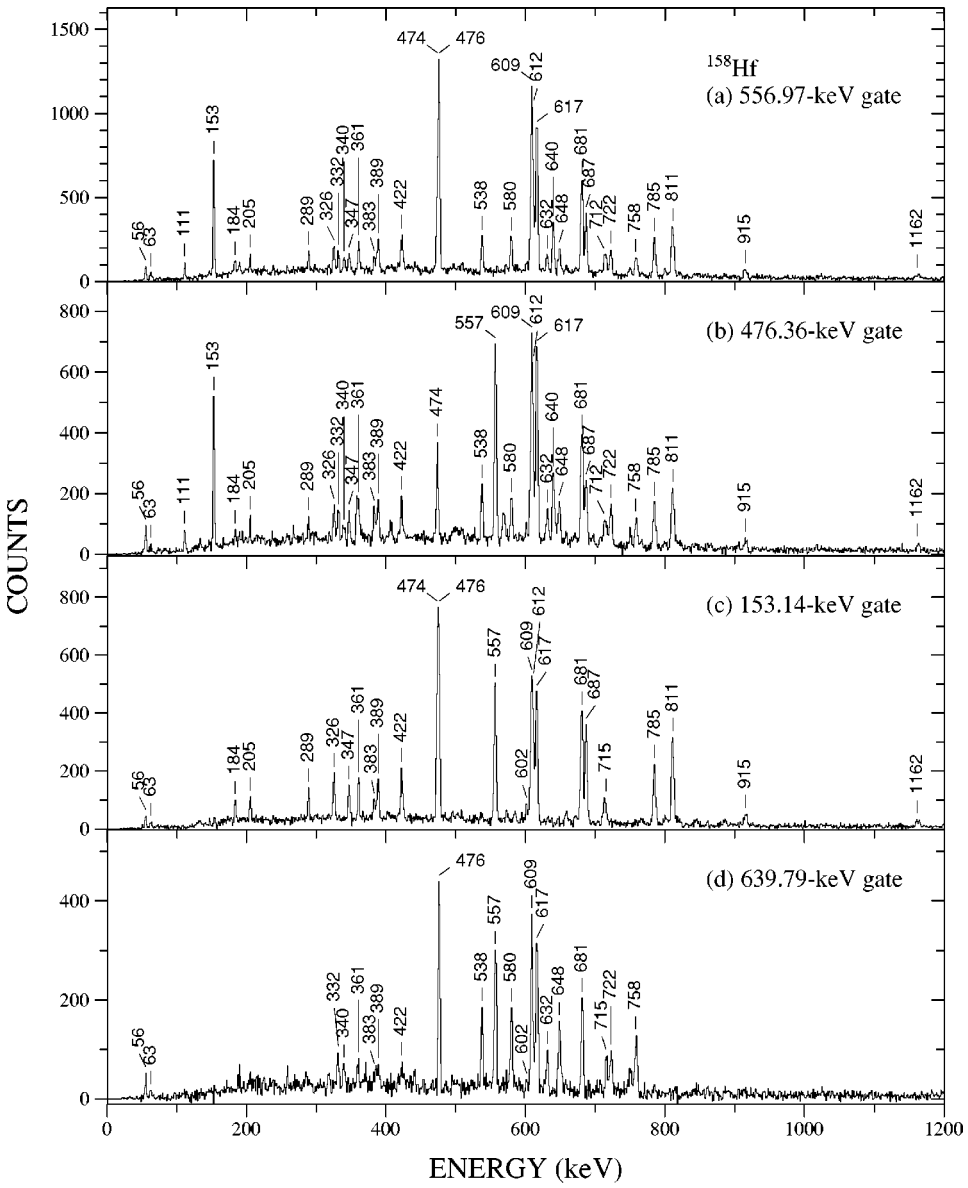

FIG. 4. Coincidence spectra gated on the (a) 556.97-, (b) 476.36-, (c) 153.14-, and (d) 639.79-keV transitions in ^{158}Hf in the matrix gated on $A=158$.

scheme in Fig. 3 is the first to be reported.

The strongest transition in Fig. 2 is at 556.97 keV; a spectrum gated on this transition in the matrix gated on $A=158$, without α-decay tagging, is shown in Fig. 4(a). The 556.97-keV transition is in coincidence with all of the other transitions identified in Fig. 2(a). The spectrum gated on the 476.36-keV low-lying transition is displayed in Fig. 4(b). Although the four low-lying transitions are similar in intensity, the 476.36-keV transition is assigned as the $2^+ \rightarrow 0^+$ transition to give the quasiband structure expected for this $N=86$ isotone.

The 153.14-keV transition connects the negative-parity, high-spin and positive-parity, low-lying yrast cascades. Angular distribution and intensity balance arguments suggest that the 153.14-keV transition is likely of stretched $E1$ character; the spectrum gated on this transition is displayed in Fig. 4(c). The negative-parity cascade becomes yrast above $10\hbar$, and is observed up to $I \gtrsim 25\hbar$ and $E_x \sim 9.1$ MeV. Above the 21^- state at 6462 keV, the negative-parity sequence becomes irregular and fragments into many branches. The transitions above the (21^-) state are weaker in intensity, and the spin and parity assignments of these states are tentative because the angular distributions of these transitions are uncertain. In the level scheme displayed in Fig. 3, a 61-keV transition is suggested. Although the intensities in the x-ray energy regions in spectra gated on specific transitions are too weak to identify this low-energy transition, a 61.3-keV transition is observed in the total projection spectrum gated on the α decay of ^{158}Hf.

Two non-yrast, positive-parity cascades in ^{158}Hf are observed up to $E_x \sim 6$ MeV and $I \sim 20^+$. One decays into the other, which then in turn decays to the yrast, positive-parity cascade via $E2$ transitions. The coincidence spectrum gated on the 639.79-keV transition is displayed in Fig. 4(d).

B. Level scheme of ^{159}Hf

^{159}Hf nuclei could be produced by the fusion of the beam and the $^{104-106}$Pd contaminants in the target. The known

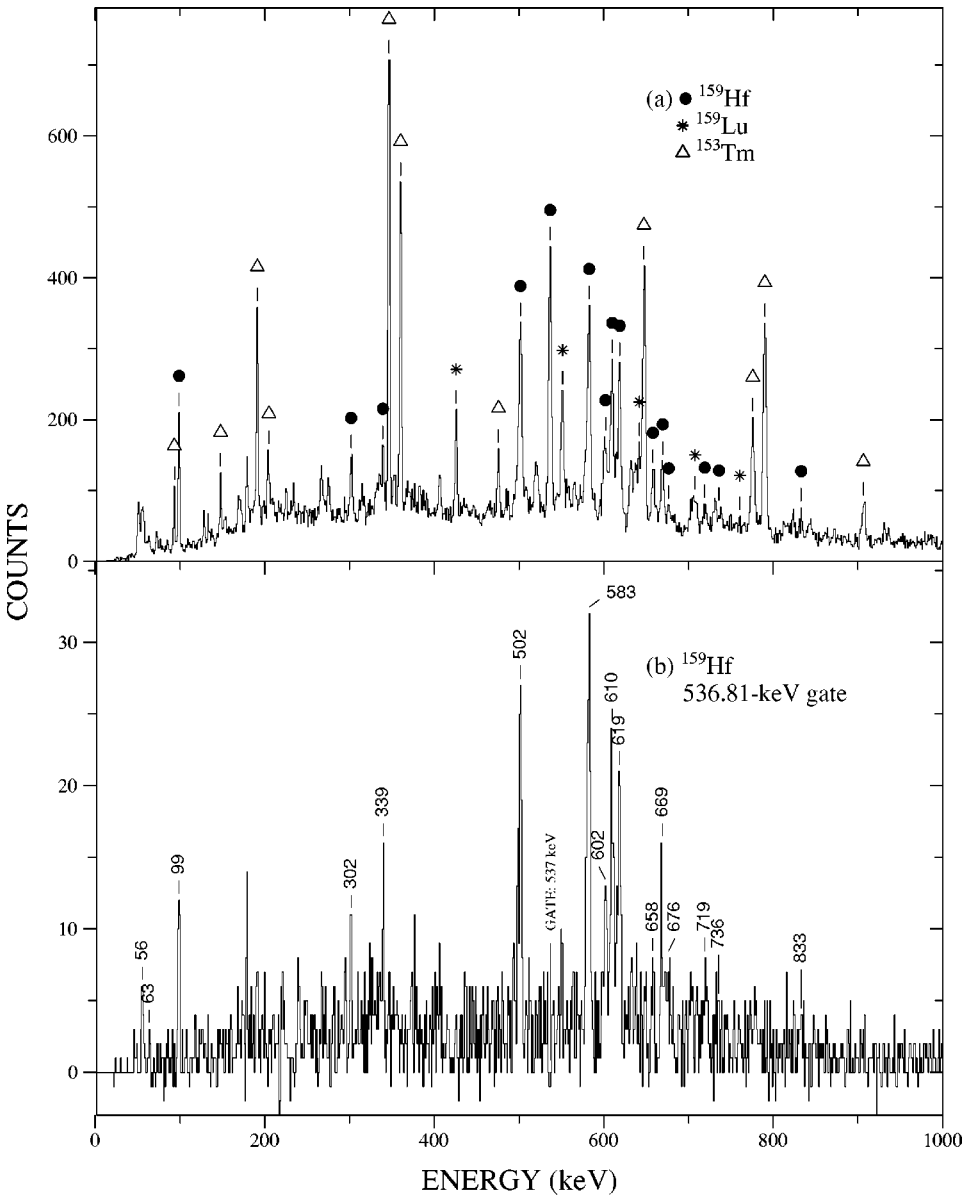

FIG. 5. (a) Total projection of the γ-ray events gated on $A=153+159$ and the α decay of the high-spin isomer in ^{159}Hf ($E_\alpha=5.098$ MeV, $t_{1/2}=5200$ ms). Transitions in ^{159}Hf, ^{153}Tm [13], and ^{159}Lu [14] are labeled. (b) Coincidence spectrum gated on the 536.81-keV transition in ^{159}Hf in the matrix gated on $A=153+159$ and the α decay associated with the isomer in ^{159}Hf.

characteristic α decay of ^{159}Hf ($E_\alpha=5.098$ MeV and $t_{1/2}=5200$ ms) [11] is identified in the present data. Note that the positions of $A=153$ and $A=159$ nuclei are nearly degenerate at the focal plane (M/Q ambiguity).

The total projection of the γ-ray events gated on $A=153+159$ and on the α decay associated with the high-spin isomer in ^{159}Hf is displayed in Fig. 5(a). The x-ray energy region is complex and indicates that more than one element is observed. In addition to ^{159}Hf, transitions correlated with ^{153}Tm [13], with the same focal plane position and similar α decay properties ($E_\alpha=5.112$ MeV [11] and $t_{1/2}=1.48$ s [15]), are identified in this spectrum.

Transitions which belong to ^{159}Lu [14] are also identified in this spectrum, although the energy of the α particles associated with the decay of the high-spin isomer in ^{159}Lu quoted in the literature [16] is 4.530 MeV. In addition, no peak at 4.530 MeV is observed in the α-energy spectrum gated on mass $=153+159$ [10]. Although an α-energy spectrum gated on mass $=153+159$ and the strongest γ-ray transitions in ^{159}Lu was carefully studied, statistics were insufficient to determine the energy of the α decay. These results suggest that a more accurate measurement of the α-decay characteristics of ^{159}Lu may be required.

Other than the transitions which have been previously assigned to ^{153}Tm [13] and ^{159}Lu [14], all of the transitions inFig. 5(a) belong to the same nucleus, with the strongest transition at 536.81 keV. A coincidence gate on the 536.81-keV transition in the matrix gated on $A=153+159$ and the α decay associated with the high-spin isomer in ^{159}Hf is shown in Fig. 5(b). The energies of the x rays in the coincidence spectrum are consistent with Hf isotopes.

The γ-γ matrix gated on $A=153+159$, as well as the matrix gated on $A=153+159$ and the α decay associated with the isomer in ^{159}Hf, were used for level scheme construction. The level scheme of ^{159}Hf in Fig. 6 is studied for the first time in the present work, although transitions in ^{159}Hf have been previously reported [12]. A summary of the γ-ray transitions is displayed in Table II. The relative inten-

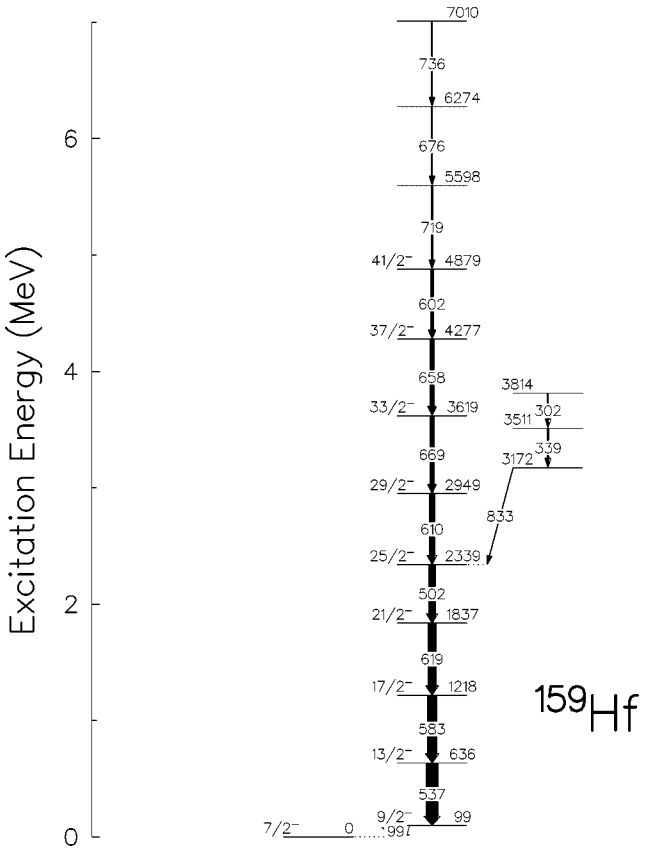

FIG. 6. Level scheme of ^{159}Hf.

sities were obtained from the coincidence spectrum gated on the 98.87-keV transition, presented in Fig. 7(a), from the matrix gated on $A=153+159$.

A negative-parity yrast cascade and a few non-yrast transitions have been identified in ^{159}Hf. The angular distribution of the 98.87-keV line indicates that it is likely of stretched dipole character. By comparing the relative intensities of the transitions in Fig. 7(a) to the total projection in Fig. 5, the 98.87-keV line is probably the $M1$ transition from the $9/2^-$ to $7/2^-$ state. This assignment is also supported by the observation that the isomer in ^{159}Hf α decays to the $7/2^-$ state in ^{155}Yb [16]. In subsequent discussions a $7/2^-$ assignment for the ^{159}Hf isomer is assumed. The non-yrast states feed the yrast band at the $25/2^-$ level. Spectra gated on the 658.05-keV transition, a member of the yrast band, and the 832.9-keV line, a non-yrast transition, are displayed in Figs. 7(b,c). Transitions at 708.1- and 782.7-keV are also observed in the coincidence spectra of the two bands, but no placements are available due to insufficient statistics.

C. Level scheme of ^{160}Hf

The positions of $A=154$ and $A=160$ nuclei are nearly degenerate at the focal plane. The γ-ray spectrum gated on $A=154+160$ and the ground-state α decay of ^{160}Hf ($E_\alpha=4778$ MeV [11] and $t_{1/2}=13$ s [17]) is displayed in Fig. 8. Although transitions have been previously observed [18], the spectrum in Fig. 8 provides a unique identification of the transitions which belong to ^{160}Hf. A γ-γ matrix gated on $A=154+160$ and the α decay of ^{160}Hf and a γ-γ matrix gated only on $A=154+160$ were constructed to establish the ^{160}Hf level scheme.

The level scheme of ^{160}Hf is displayed in Fig. 9. The spectrum gated on the 389.40-keV, $2^+\rightarrow0^+$ transition is displayed in Fig. 10(a). The summary of the transitions is given in Table III. The relative intensities of the transitions were obtained from the sum of coincidence spectra gated on the 389.40- ($2^+\rightarrow0^+$) and 508.86-keV ($4^+\rightarrow2^+$) transitions because this summed spectrum is not contaminated by other reaction channels and has higher statistics than the α-tagged

TABLE II. Energies, relative intensities, a_2 coefficients, and placements of γ-ray transitions in ^{159}Hf. Spin and parity assignments are based on angular distributions.

Energy (keV)	Intensity %	a_2	Mult.	E_x (keV) E_i	E_f	Assignment I_i^π	→	I_f^π
98.87(10)	394(68)	−0.28(10)	$M1$	99	0	$9/2^-$	→	$7/2^-$
302.13(12)	92(10)			3511	3172			
339.49(11)	130(11)			3814	3511			
501.84(11)	574(92)	0.38(7)	$E2$	2339	1837	$25/2^-$	→	$21/2^-$
536.81(10)	≡1000	0.24(4)	$E2$	636	99	$13/2^-$	→	$9/2^-$
582.73(12)	768(93)	0.30(7)	$E2$	1218	636	$17/2^-$	→	$13/2^-$
601.99(12)	260(48)	0.17(7)	$E2$	4879	4277	$41/2^-$	→	$37/2^-$
610.0(11)	444(73)	0.37(3)	$E2$	2949	2339	$29/2^-$	→	$25/2^-$
618.78(10)	699(113)	0.49(4)	$E2$	1837	1218	$21/2^-$	→	$17/2^-$
658.05(11)	348(58)	0.34(10)	$E2$	4277	3619	$37/2^-$	→	$33/2^-$
669.46(11)	363(61)	0.45(6)	$E2$	3619	2949	$33/2^-$	→	$29/2^-$
676.5(2)	90(21)			6274	5598			
708.1(3)*	61(13)							
719.17(14)	127(26)			5598	4879			
735.6(2)	90(20)			7010	6274			
782.7(3)*	73(13)							
832.9(2)	49(8)			3172	2339			

*Not placed.

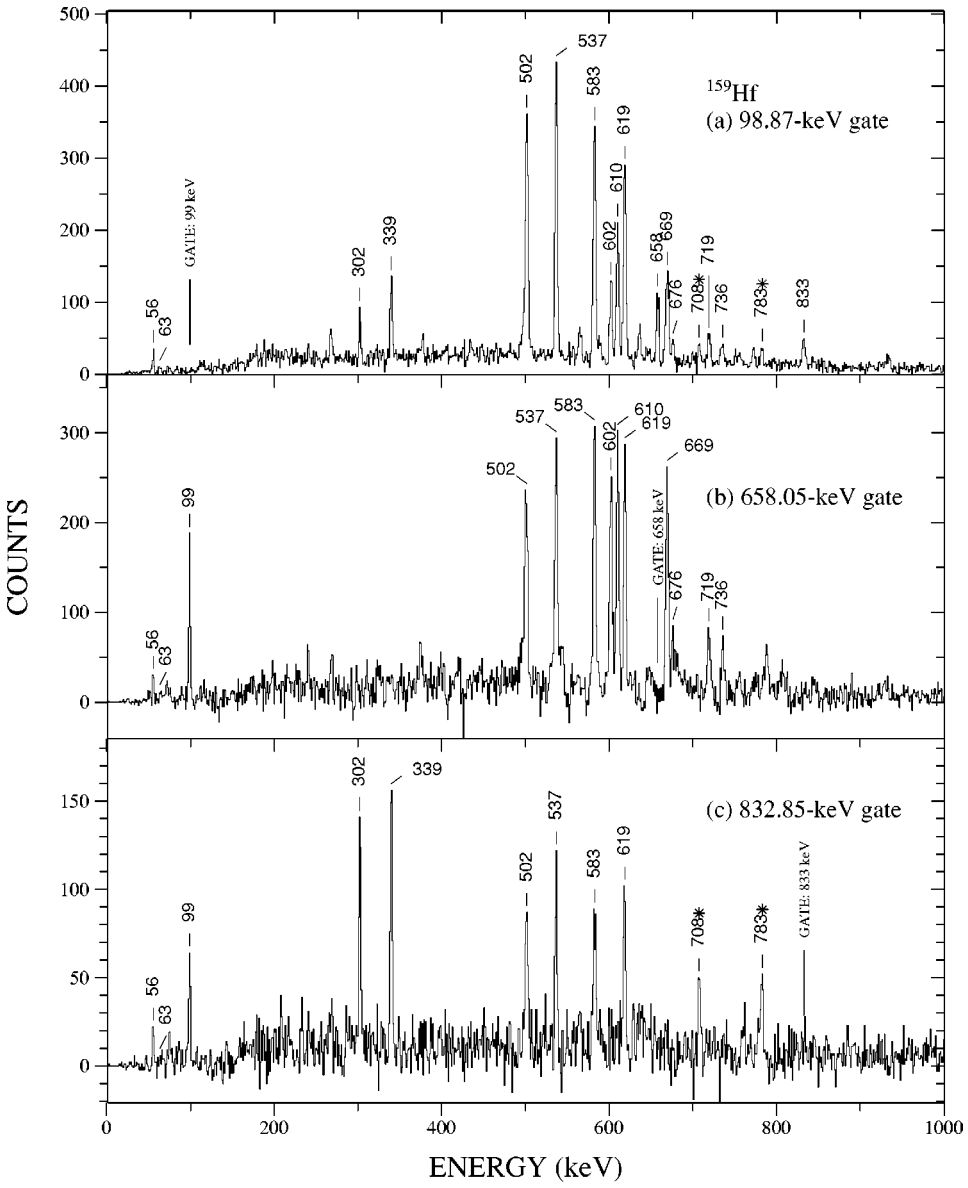

FIG. 7. Coincidence spectra gated on the (a) 98.87-, (b) 658.05-, and (c) 832.9-keV transitions in ^{159}Hf from the matrix gated on $A=153+159$. The transitions marked with an asterisk have not been placed in the level scheme.

total projection in Fig. 8. The spin and probable parity assignments were based on the angular distributions of the transitions and on intensity balance arguments. The current level scheme confirmed the previous work [18] in which the odd-spin, negative-parity band was observed up to $\sim$7.0 MeV and the even-spin, positive-parity band was observed up to $\sim$5.4 MeV. The even-spin, negative-parity band is new in the present measurement; the members of this cascade had been previously reported [18], but were not placed.

Above the 10^+ state at 2815 keV, the odd-spin, negative-parity cascade becomes the yrast band. This cascade decays to the low-lying positive-parity yrast band via $E1$ transitions. Coincidence gates on the 211.48- and 566.24-keV $E1$ γ rays, which correspond to the $11^-\rightarrow 10^+$ and $9^-\rightarrow 8^+$ transitions, are shown in Fig. 10(b) and (c), respectively. The 11^- state at 3026 keV also decays to the non-yrast 9^- level at 2748 keV. One new transition has been added to the top of the odd-spin, negative-parity cascade. The 216.57-keV transition connects the even-spin, negative-parity cascade to the 9^- state at 2748 keV. The members of the even-spin, negative-parity band, as well as the transitions fed by the 9^- level at 2714 keV, are identified in the spectrum gated on the 566.24-keV transition. The even-spin negative-parity band also decays to the odd-spin, negative-parity band via the 250.42-keV transition.

IV. DISCUSSION

A. Level structures of ^{158}Hf and ^{160}Hf

1. Low-spin structure

The systematics of the excitation energies of the low-lying yrast states in the even-A Hf isotopes is shown in Fig. 11. The structure changes from deformed rotational in ^{168}Hf ($N=96$) to single particle in ^{156}Hf ($N=84$), with transitional character for ^{158,160}Hf. The nature of the low-lying states in Hf isotopes can be illustrated further by examining

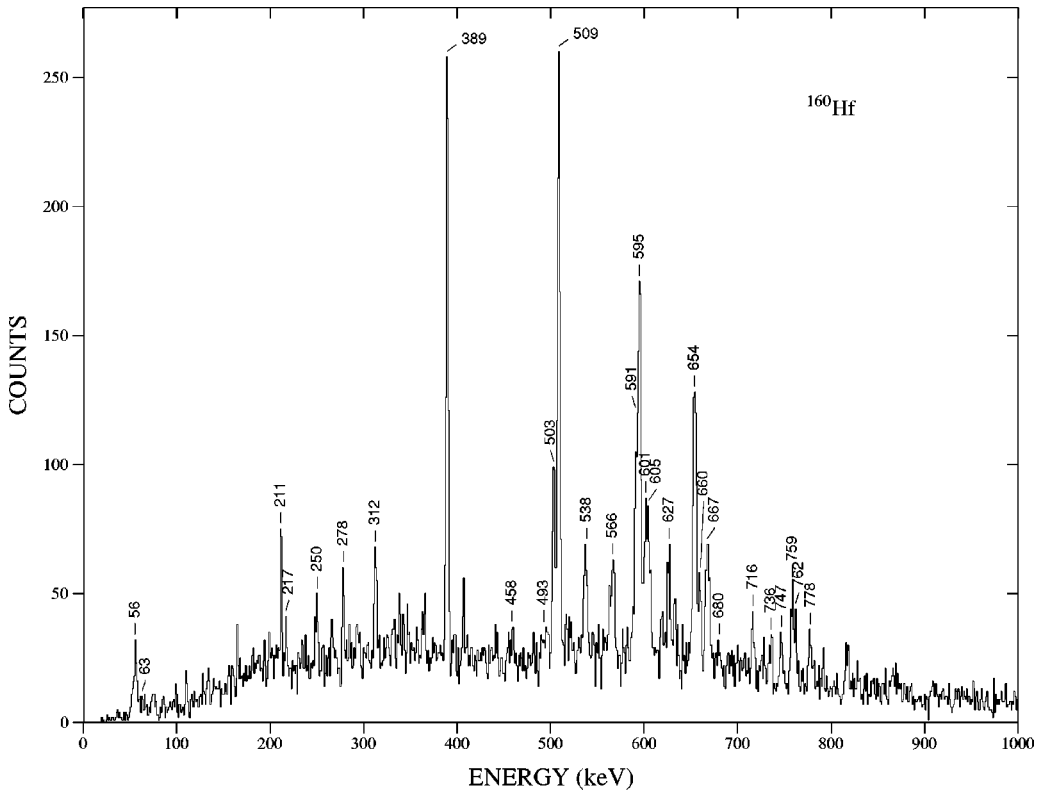

FIG. 8. Total projection of the γ-ray events gated on $A=154+160$ and the α decay of ^{160}Hf ($E_\alpha=4.778$ MeV, $t_{1/2}=13$ s).

the ratios of the excitation energies, $R_{4/2}=E(4_1^+)/E(2_1^+)$ and $R_{6/4}=E(6_1^+)/E(4_1^+)$, as a function of neutron number, as displayed in Fig. 12. The theoretical values for $R_{4/2}$ and $R_{6/4}$ for a harmonic vibrator are 2.00 and 1.50, respectively, and for a rigid rotor are 3.33 and 2.00, respectively. Both experimental ratios decrease gradually from near rotor values in ^{168}Hf to near vibrational values in ^{158}Hf and to values below those expected for a vibrator in ^{156}Hf.

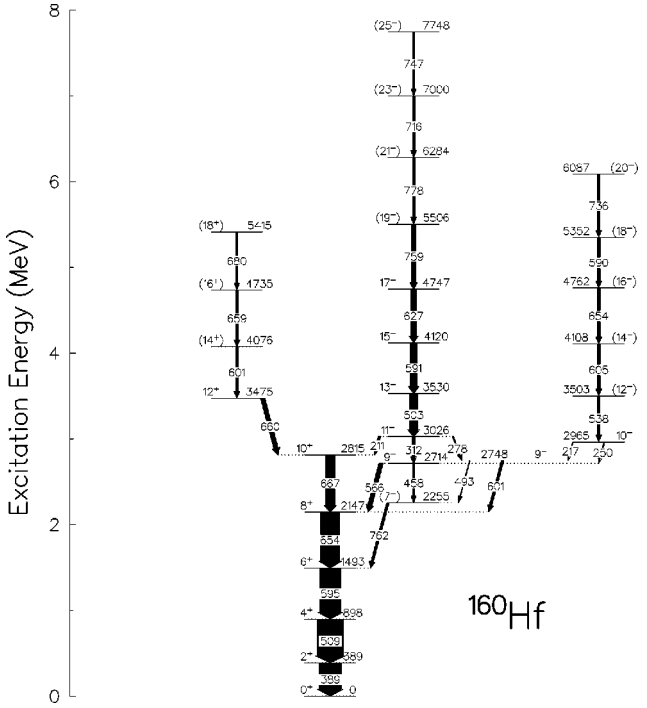

FIG. 9. Level scheme of ^{160}Hf.

The systematics of the energy ratios $R_{4/2}$ and $R_{6/4}$ for the even-A, $N=86,88$ isotones are shown in Fig. 13. These ratios are essentially constant for the $N=88$ isotones with $Z \geqslant 68$.

The increase in the attractive proton-neutron interaction has been introduced to explain the onset of deformation for $N>88$, $Z \geqslant 64$ nuclei in Ref. [26]. For $N<90$, the neutrons predominantly occupy the $f_{7/2}$ orbital, which has a relatively small overlap with the protons in the $h_{11/2}$ orbital and, therefore, results in a smaller proton-neutron interaction. For $N>88$, the neutrons have a larger occupation probability of the $h_{9/2}$ orbital, especially for the $Z=72$ nuclei examined in this work, in which the energy difference between the $\nu f_{7/2}$ and $\nu h_{9/2}$ orbitals is small. The strong attractive interaction between protons and neutrons in the spin-orbit partner orbitals, $\pi h_{11/2}$ and $\nu h_{9/2}$, also lowers the energy of the $\pi h_{11/2}$ orbital, which decreases the subshell gap at $Z=64$. For $N>88$, it is more appropriate to invoke the full $Z=50-82$ shell to determine the number of valence protons. The increase in the number of valence protons for $N>88$ increases the overall proton-neutron interaction, which drives the nucleus to prolate quadrupole deformation. Although the energy difference between $\nu f_{7/2}$ and $\nu h_{9/2}$ excitations is only 99 keV in ^{159}Hf, the energy ratios in the ^{158,160}Hf cores are similar to those in more stable isotones. This suggests that a possible higher occupation probability of the $\nu h_{9/2}$ orbital does not increase the collectivity when compared to lighter

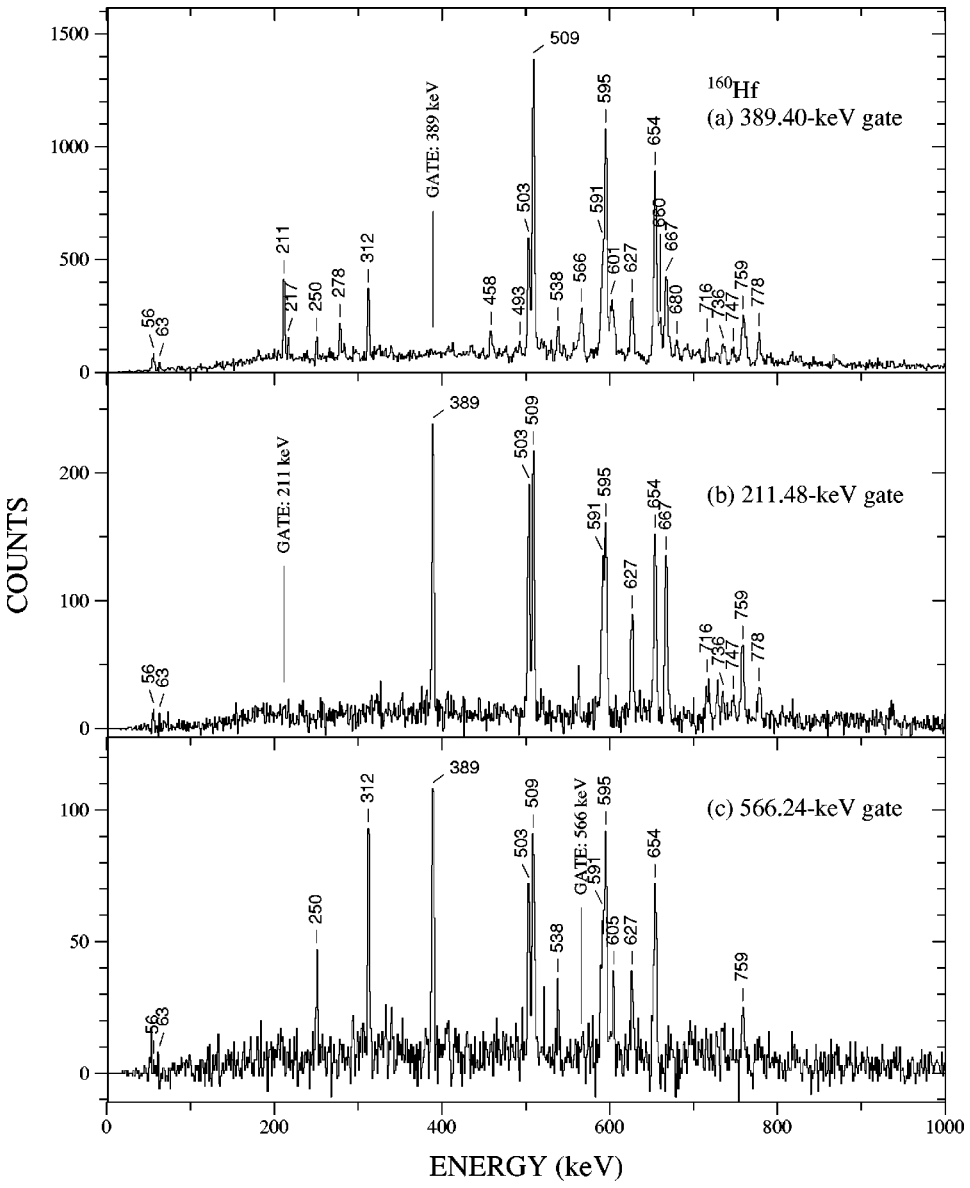

FIG. 10. Coincidence spectra gated on the (a) 389.40-, (b) 211.48-, and (c) 566.24-keV transitions in ^{160}Hf in the matrix gated on $A=154+160$.

isotones for which the separation between $\nu f_{7/2}$ and $\nu h_{9/2}$ orbitals is larger.

The systematics of the low-lying states in the even-Z, $N=86$ isotones is shown in Fig. 14. The almost constant energy spacings between the $0^+,2^+,4^+$, and 6^+ states suggests predominantly vibrational excitations of neutrons, with proton contributions that do not change as the number of valence protons increases. For the low-spin states, the dominant component would be $(\nu f_{7/2})^2$. The 8^+ state requires $(\nu f_{7/2}h_{9/2})$ or $(\nu h_{9/2})^2$ components. Isomeric 11^- states are observed in all of the even-A, $N=86$ isotones [22–25] with $64\geqslant Z\geqslant 72$; the configuration is possibly $\nu h_{9/2}i_{13/2}$. The 11^- to 17^- sequences observed in all of the even-A, $N=86$ isotones can be generated by coupling $(\nu f_{7/2})^2_{0^+,2^+,4^+,6^+}$ to the configuration of the 11^- isomer. In ^{158}Hf this negative-parity sequence has irregular spacings, which are similar to those observed for the $(\nu f_{7/2})^2$ configurations in $N=84$ isotones [19]. In contrast, the positive-parity cascade built on the 10^+_2 state in ^{158}Hf, displayed in Fig. 3, has the more equal energy spacings which would characterize a vibrational, collective structure.

In ^{160}Hf, as displayed in Fig. 9, the odd-spin, negative-parity cascade becomes yrast above $10\hbar$. The low-spin members of this cascade are probably built on a 3^-, octupole vibrational band, which is crossed at higher spins by the $\nu h_{9/2}i_{13/2}$ two-quasiparticle configuration, which is isomeric in the $N=86$ isotones [22–25].

2. High-spin structure

The high angular momentum properties of the Hf isotopes can be studied by comparing the aligned spins as a function of rotational frequency. The aligned spins for the positive-parity bands in the even-A, $N=86-96$ Hf isotopes are shown in Fig. 15(a). The aligned spins display a backbend above $10\hbar$ due to the alignment of two $i_{13/2}$ neutrons at $\hbar\omega\sim 0.25-0.35$ MeV. The sharpness of the backbend in the Hf isotopes first increases with neutron number from ^{158}Hf with $N=86$ to a maximum in ^{164}Hf with $N=92$, then de-

TABLE III. Energies, relative intensities, a_2 coefficients, and placements of γ-ray transitions in ^{160}Hf. Spin-parities in parentheses are tentative.

Energy (keV)	Intensity %	a_2	Mult.	E_x (keV) E_i	E_f	Assignment I_i^π	→	I_f^π
211.48(10)	99(19)	-0.40(6)	$E1$	3026	2815	11^-	→	10^+
216.57(13)	22(6)	-0.97(22)	$M1$	2965	2748	10^-	→	9^-
250.42(13)	28(7)	-0.32(11)	$M1$	2965	2714	10^-	→	9^-
278.21(12)	49(11)	0.21(17)	$E2$	3026	2748	11^-	→	9^-
312.30(11)	111(21)	0.26(5)	$E2$	3026	2714	11^-	→	9^-
389.40(10)	842(106)	1.15(3)	$E2$	389	0	2^+	→	0^+
458.47(13)	66(14)		$(E2)$	2714	2255	9^-	→	(7^-)
492.7(3)	32(8)		$(E2)$	2748	2255	9^-	→	(7^-)
503.49(10)	324(53)	0.21(17)	$E2$	3530	3026	13^-	→	11^-
508.86(10)	$\equiv$1000		$E2$	898	389	4^+	→	2^+
538.5(2)	90(17)		$(E2)$	3503	2965	(12^-)	→	10^-
566.24(12)	166(30)	-0.74(22)	$E1$	2714	2147	9^-	→	8^+
589.7(2)	$<$110		$(E2)$	5352	4762	(18^-)	→	(16^-)
590.76(12)	284(49)	0.45(9)	$E2$	4120	3530	15^-	→	13^-
595.09(10)	812(126)	0.22(5)	$E2$	1493	898	6^+	→	4^+
600.6(5)	}179(34)		$E1$	2748	2147	9^-	→	8^+
601.5(5)			(E2)	4076	3475	(14^+)	→	12^+
605.0(2)	144(29)	0.10(7)	$E2$	4108	3503	(14^-)	→	(12^-)
626.63(11)	218(37)	0.37(15)	$E2$	4747	4120	17^-	→	15^-
653.9(2)	$<$110		$(E2)$	4762	4108	(16^-)	→	(14^-)
654.13(10)	715(110)	0.29(6)	$E2$	2147	1493	8^+	→	6^+
658.7(5)	$<$110		$(E2)$	4735	4076	(16^+)	→	(14^+)
660.12(13)	167(30)	0.22(18)	$E2$	3475	2815	12^+	→	10^+
667.25(11)	350(56)	0.24(7)	$E2$	2815	2147	10^+	→	8^+
680.4(2)	74(15)		$(E2)$	5415	4735	(18^+)	→	(16^+)
716.4(2)	103(20)	0.51(13)	$E2$	7000	6284	(23^-)	→	(21^-)
735.58(15)	88(17)	0.24(9)	$E2$	6087	5352	(20^-)	→	(18^-)
747.2(2)	59(13)		$(E2)$	7748	7000	(25^-)	→	(23^-)
758.8(2)	183(38)		$(E2)$	5506	4747	(19^-)	→	17^-
762.0(2)	99(26)		$(E1)$	2255	1493	(7^-)	→	6^+
778.10(13)	102(20)	0.41(13)	$E2$	6284	5506	(21^-)	→	(19^-)

creases with neutron number to ^{168}Hf with $N=96$. This observation can be explained by the predicted oscillating behavior with neutron number of the interaction matrix element [27] between the ground band and the $(\nu i_{13/2})^2$ band. Therefore, the increase in the degree of backbending from ^{158}Hf to ^{164}Hf indicates a decrease in strength of the interaction between the two bands. For the two 10^+ states in ^{158}Hf in Fig. 3 separated by only 42 keV, the interaction is at most 21 keV, assuming two-state mixing [28].

The strength of the interaction as a function of proton number can also be studied by plotting the aligned spin as a function of proton number for the $N=88$ isotones, as shown in Fig. 16(a). The observation that the degree of backbending is stronger in ^{156}Er and ^{158}Yb and weaker in ^{160}Hf indicates that the interaction between the ground-state and excited bands is stronger in ^{160}Hf. This dependency of the interaction on the proton number can be reproduced by the calculations of Ref. [30], if a relatively large hexadecapole deformation is assumed.

The aligned spin as a function of proton number for the even-even $N=86$ isotones is displayed in Fig. 16(b). The irregular relation between the aligned spin and the rotational frequency for these nuclei indicates that the high-spin states are generated by the alignment of the spins of individual nucleons, rather than by collective rotational motion, as suggested in the $N\geqslant 88$ isotones. Hence, the $N=86$ isotones are likely spherical or only slightly deformed nuclei.

At very high spin, collective excitations are expected to be limited because of the finite angular momentum that can be generated by the valence particles, the phenomenon of band termination. The excitation energies, after subtraction of a rotational term, for the $N=88$ isotones and ^{158}Hf are displayed in Fig. 17. The reference rotational parameter of 7 keV was chosen from previous work [6,31] to highlight the rotational motion in the 20–30 $\hbar$ region.

The dramatic decrease in Fig. 17 of energy as a function of spin, a signature of band termination, has been observed above $30\hbar$ for the high-spin states in the $N=88$ isotones [5,6,31]. Lifetime measurements of the high-spin states in ^{154}Dy [5] have shown a series of structural changes along the yrast line, including a dramatic decrease in collectivity near $36\hbar$. Because the present experiment was designed to study

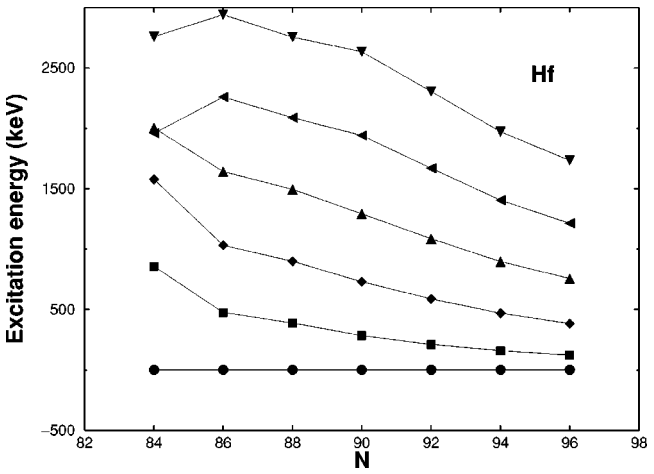

FIG. 11. Systematics of the low-lying yrast states in the even-*A* Hf isotopes. Data are taken from Refs. [3,4,19,20] and the present work.

the $N=84$ isotones near $Z=72$, rather than to perform a high-spin study of ^{158,160}Hf, the level schemes of ^{158,160}Hf could only be extended to $I\sim 25\hbar$ in the present work, well below $30\hbar$, above which the decrease in collectivity could be observed. In Fig. 3, the γ-ray strength in ^{158}Hf above $21\hbar$ is fragmented into several parallel cascades, a pattern which is characteristic of excitations in which the $N=82$ core is broken. Also, for the yrast levels at the highest spin in the $N=86$ ^{158}Hf, it appears that the energy as a function of spin does decrease, similar to what is observed above $35\hbar$ in ^{158}Yb. It would be of interest to extend to higher spins the level scheme of ^{158}Hf to determine if this decrease in energies persists, or if the present observations are only an indication of the irregular structure as a function of angular momentum expected in an essentially spherical nucleus.

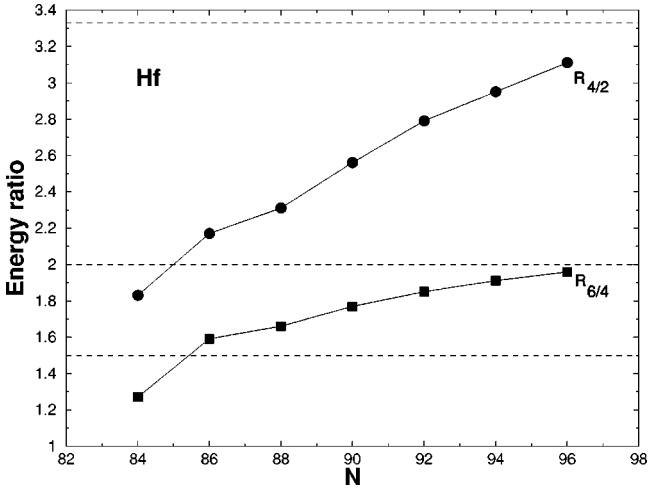

FIG. 12. Systematics of the energy ratios $R_{4/2}$ and $R_{6/4}$ as a function of neutron number in the Hf isotopes. Data are taken from Refs. [3,4,19,20] and the present work. The values for a harmonic vibrator are 2.00 and 1.50, respectively, and for a rigid rotor are 3.33 and 2.00, respectively, as indicated by dashed lines.

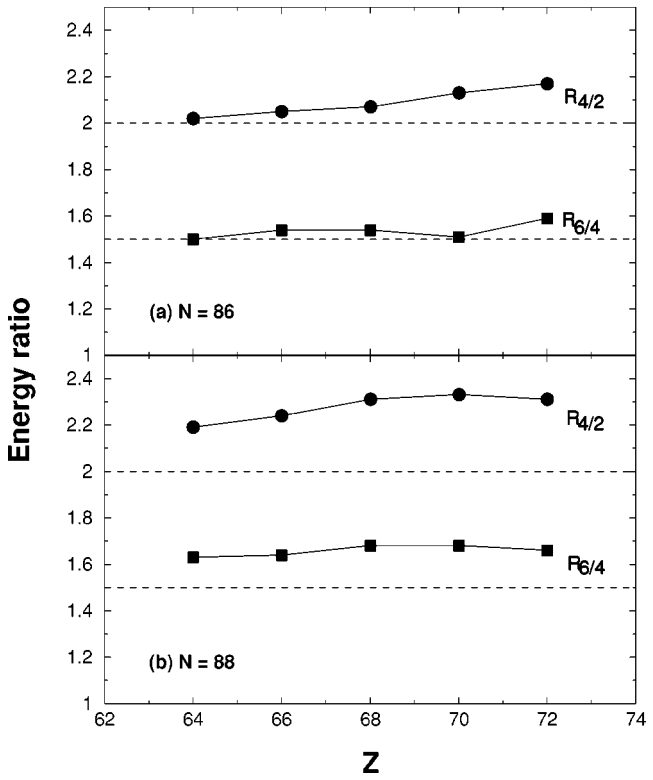

FIG. 13. Systematics of the energy ratios $R_{4/2}$ and $R_{6/4}$ as a function of proton number for the even-even (a) $N=86$ and (b) $N=88$ isotones. The values for a harmonic vibrator are indicated by dashed lines. Data are taken from Refs. [5–7,21–25] and the present work.

B. Level structure of ^{159}Hf

The properties of the yrast states observed in ^{159}Hf are different from those observed in the even-Z, $N=87$ isotones [32,33]. Although $7/2^-$ isomers based on $f_{7/2}$ neutrons are observed in all of the isotones, the yrast cascades in ^{153}Dy and ^{155}Er are built upon $13/2^+$, $\nu i_{13/2}$ isomers which decay to the $11/2^-$ states located above the $\nu f_{7/2}$ isomers. In con-

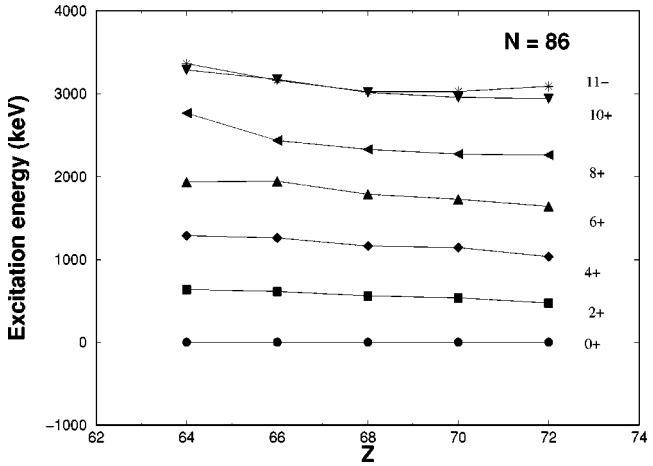

FIG. 14. Systematics of the low-lying states in the even-Z, $N=86$ isotones from ^{150}Gd to ^{158}Hf. Data are taken from Refs. [22–25] and the present work.

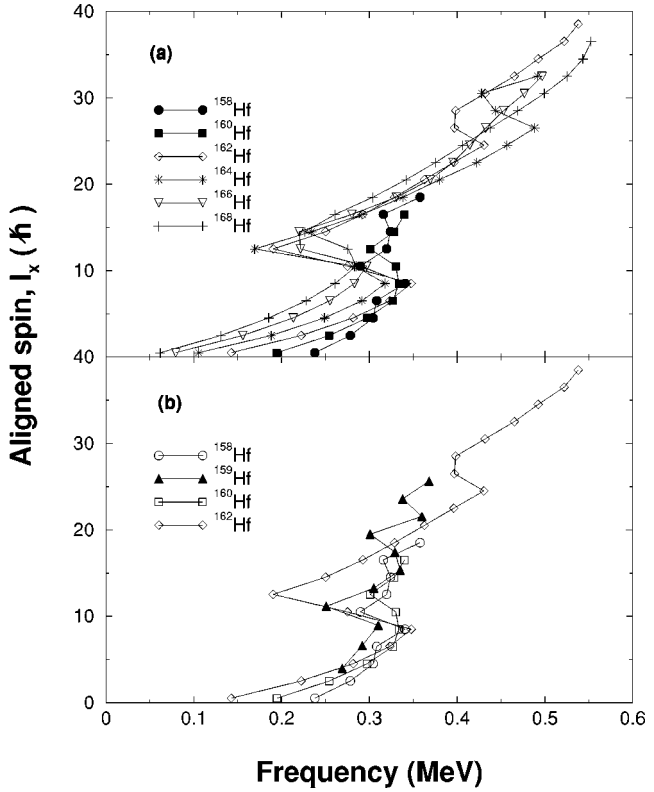

FIG. 15. Aligned spins I_x as a function of rotational frequency, $\hbar\omega$, for (a) the even-A Hf isotopes and (b) ^{158,159,160,162}Hf. $K=0$ and $K=9/2$ were assumed for the yrast cascades in even- and odd-mass Hf nuclei, respectively. Data are taken from Refs. [3,4,20] and the present work.

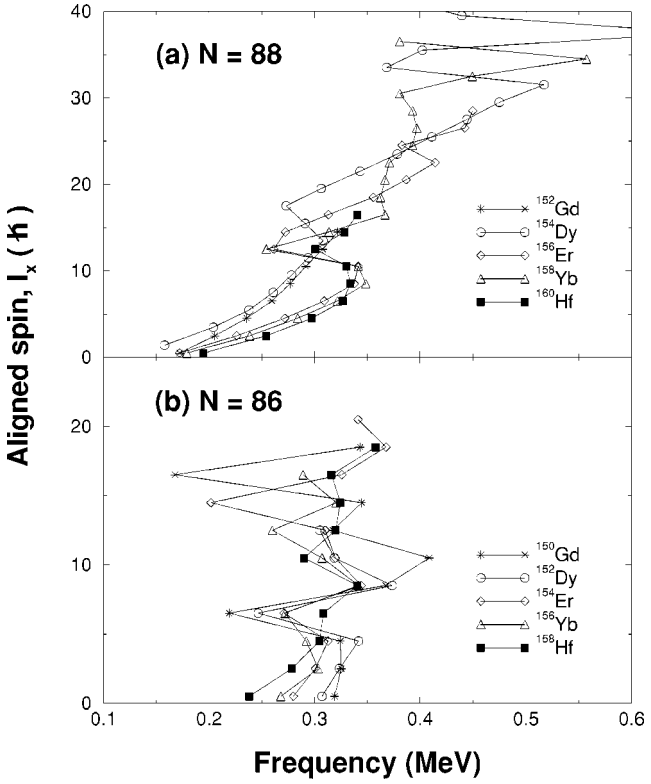

FIG. 16. Aligned spins I_x as a function of the rotational frequency $\hbar\omega$ for the (a) even-Z, $N=88$ and (b) even-Z, $N=86$ isotones. Data are taken from Refs. [5,6,21–25,29] and the present work.

trast, the yrast structure in ^{159}Hf is built on the $\nu h_{9/2}$ configuration which is only 99 keV above the $\nu f_{7/2}$ isomer. The level structure of the $Z=70$, $N=85$ isotone ^{157}Yb has not been published. The yrast excitations built on the $\nu i_{13/2}$ isomers in ^{153}Dy and ^{155}Er have energy spacings more characteristic of rotational motion, while those built on the $\nu h_{9/2}$ configuration in ^{159}Hf have more vibration-like spacings. It would be of interest to search for excitations built on the $\nu i_{13/2}$ configuration in ^{159}Hf to determine if these excitations are associated with the same deformation as those observed in the lighter isotones.

The aligned spins as a function of rotational frequency for the positive-parity bands in ^{158,160,162}Hf and the yrast band in ^{159}Hf are displayed in Fig. 15(b). The alignment behavior for ^{159}Hf appears to be intermediate between that of ^{160}Hf and ^{162}Hf. This could suggest that the occupation of the $\nu h_{9/2}$ orbital in ^{159}Hf, and the subsequent alignment of neutrons in the $i_{13/2}$ orbital, allow for a more collective structure in ^{159}Hf, than occurs in ^{160}Hf, with lower occupation of the $\nu h_{9/2}$ orbital in the ground-state configuration.

V. SUMMARY

Level schemes up to $E_x \sim 9.1$ MeV and $I \gtrsim 25\hbar$ in ^{158}Hf, up to $E_x \sim 7.0$ MeV and $I \gtrsim 41/2\hbar$ in ^{159}Hf, and up to $E_x \sim 7.7$ MeV and $I \gtrsim 25\hbar$ in ^{160}Hf have been presented. For ^{158}Hf and ^{159}Hf, the level schemes are presented for the first time, while for ^{160}Hf, an even-spin negative-parity band has been added to the previous work [18].

The $\nu f_{7/2}$ configuration has been assigned to the ground state in ^{159}Hf, with the yrast cascade built on the $\nu h_{9/2}$ state at 99 keV. This structure is different from those observed in the even-Z, $N=87$ isotones, ^{153}Dy [32] and ^{155}Er [33], in which the yrast cascades are rotational bands built upon the

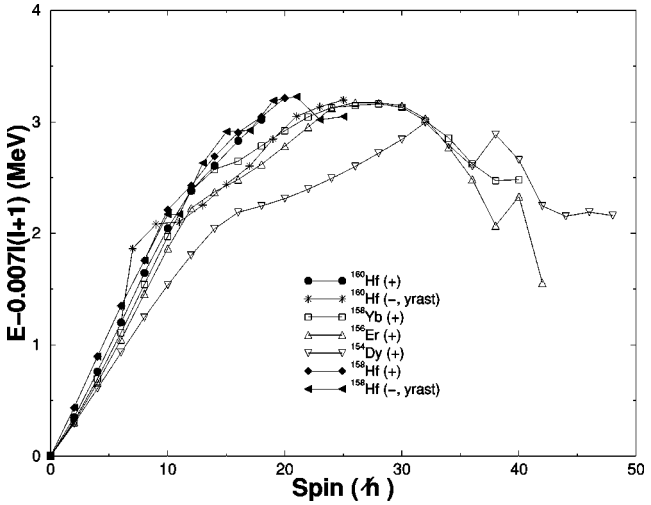

FIG. 17. Excitation energies of the yrast states as a function of spin for the even-Z, $N=88$ isotones and ^{158}Hf. A rigid rotor reference has been subtracted. Data are taken from Refs. [5–7] and the present work.

$\nu i_{13/2}$ configuration. This difference in yrast structure between ^{159}Hf and the lighter $N=87$ isotones is attributed to the lowering of the $\nu h_{9/2}$ orbital as the number of valence protons increases due to the attractive interaction between $\nu h_{9/2}$ and $\pi h_{11/2}$ configurations. It would be important to study the excitations in ^{157}Yb to complete the $N=87$ systematics, and to search, in ^{159}Hf, for excitations built upon the $\nu i_{13/2}$ configuration, which is expected to be deformed based on the systematics of the lighter $N=87$ isotones.

The present work extends the study of high-spin phenomena in neutron-deficient Hf isotopes towards the proton-dripline. The low-lying level structures of ^{158,160}Hf follow the trends observed in more stable isotopes and isotones. In particular, a sharp backbend, attributed to the alignment of a pair of $i_{13/2}$ neutrons, is observed in ^{158,159,160}Hf at rotational frequencies similar to those observed in heavier isotopes. The weak interaction between the ground-state and aligned configurations, at most 21 keV in ^{158}Hf, assuming two-state mixing, suggests small components of $(\nu i_{13/2})^2$ in the ground state.

Although band termination near $I=30-40\,\hbar$ has been previously observed in the even-Z, $N=88$ isotones, e.g., Refs. [6,31], ^{158}Hf and ^{160}Hf were only populated up to $I\sim 25\hbar$. Therefore, it is difficult to conclude whether the same phenomenon is observed in these Hf nuclei.

The population of high-spin states in $^{158-160}$Hf was limited in the present measurement; a future study to extend the level schemes to higher angular momentum in these nuclei should be possible with $^{104-106}$Pd+^{58}Ni reactions, at a slightly higher beam energy and with targets enriched in these Pd isotopes. Lifetime measurements, which provide a direct probe of the collectivity, would also be important to ascertain the evolution of shape changes along the yrast line. However, such measurements are very difficult in these neutron-deficient nuclei populated with small cross sections in reactions with a plethora of available channels.

ACKNOWLEDGMENTS

This work was supported in part by U.S. National Science Foundation and the Department of Energy–Nuclear Physics Division under Contract Nos. W-31-109-ENG-38 and DE-AC03-76SF00098.

[1] Y. A. Akovali, K. S. Toth, A. L. Goodman, J. M. Nitschke, P. A. Wilmarth, D. M. Moltz, M. N. Rao, and D. C. Sousa, Phys. Rev. C **41**, 1126 (1990).
[2] C. T. Zhang *et al.*, Phys. Rev. C **54**, R1 (1996).
[3] H. Hübel, M. Murzel, E. M. Beck, H. Kluge, A. Kuhnert, K. H. Maier, J. C. Bacelar, M. A. Deleplanque, R. M. Diamond, and F. S. Stephens, Z. Phys. A **329**, 289 (1988).
[4] K. P. Blume *et al.*, Nucl. Phys. **A464**, 445 (1987).
[5] W. C. Ma *et al.*, Phys. Rev. Lett. **61**, 46 (1988).
[6] F. S. Stephens, M. A. Deleplanque, R. M. Diamond, and A. O. Macchiavelli, Phys. Rev. Lett. **54**, 2584 (1985).
[7] C. Baktash *et al.*, Phys. Rev. Lett. **54**, 978 (1985).
[8] K. Y. Ding *et al.* (in preparation).
[9] C. N. Davids *et al.*, Nucl. Instrum. Methods Phys. Res. B **70**, 358 (1992).
[10] K. Y. Ding, Ph.D. dissertation, Rutgers University, 1999.
[11] R. Page, P. J. Woods, R. A. Cunningham, T. Davinson, N. J. Davis, A. N. James, K. Livingston, P. J. Sellin, and A. C. Shotter, Phys. Rev. C **53**, 660 (1996).
[12] G. D. Dracoulis, B. Fabricius, P. M. Davidson, A. O. Macchiavelli, J. Oliviera, J. Burde, F. Stephens, and M. A. Deleplanque, in Proceedings of the International Conference on Nuclear Structure at High Angular Momentum, Ottawa, 1992 (unpublished), p. 94.
[13] C. T. Zhang, P. Kleinheinz, M. Piiparinen, R. Collatz, T. Lönnroth, G. Sletten, and J. Blomqvist, Z. Phys. A **348**, 249 (1994).
[14] Y. Ma, H. Sun, Y. Liu, S. Wen, H. Zheng, S. Li, G. Li, G. Yuan, P. Weng, and C. Yang, J. Phys. G **21**, 937 (1995).
[15] D. Schardt *et al.*, in *Proceedings of the 5th International Conference on Nuclei Far From Stability*, edited by Ian S. Towner, Rosseau Lake, Canada, 1987, AIP Conf. Proc. No. 164 (AIP, New York, 1988), p. 477.
[16] *Table of Isotopes*, 8th ed., edited by R. B. Firestone, V. S. Shirley, C. M. Baglin, S. Y. F. Chu, and J. Zipkin (Wiley, New York, 1996).
[17] E. Hagberg, X. J. Sun, V. T. Koslowsky, H. Schmeing, and J. C. Hardy, Phys. Rev. C **45**, 1609 (1992).
[18] M. Murzel *et al.*, Nucl. Phys. **A516**, 189 (1990).
[19] D. Seweryniak *et al.*, in Proceedings of the Conference on Nuclear Structure at the Limits, 1996 (unpublished), p. 247.
[20] R. Chapman *et al.*, Phys. Rev. Lett. **51**, 2265 (1983).
[21] D. R. Zolnowski, M. B. Hughes, J. Hunt, and T. T. Sugihara, Phys. Rev. C **21**, 2556 (1980).
[22] C. Baktash, in *Proceedings of the Conference on High Angular Momentum Properties of Nuclei, Oak Ridge, Tennessee* (Harwood Academic, New York, 1983), p. 207.
[23] B. M. Nyakó, J. Simpson, P. J. Twin, D. Howe, P. D. Forsyth, and J. F. Sharpey-Schafer, Phys. Rev. Lett. **56**, 2680 (1986).
[24] C. Schuck, M. A. Deleplanque, R. M. Diamond, F. S. Stephens, and J. Dudek, Nucl. Phys. **A496**, 385 (1989).
[25] C. J. Lister, D. Horn, C. Baktash, E. der Mateosian, O. C. Kistner, and A. W. Sunyar, Phys. Rev. C **23**, 2078 (1981).
[26] R. F. Casten, D. D. Warner, D. S. Brenner, and R. L. Gill, Phys. Rev. Lett. **47**, 1433 (1981).
[27] R. Bengtsson and S. Frauendorf, Nucl. Phys. **A314**, 27 (1979).
[28] R. F. Casten, *Nuclear Structure from a Simple Perspective* (Oxford University, Oxford, 1990).
[29] S. B. Patel, F. S. Stephens, J. C. Bacelar, E. M. Beck, M. A. Deleplanque, R. M. Diamond, and J. E. Draper, Phys. Rev. Lett. **57**, 62 (1986).
[30] A. Faessler, M. Ploszajczak, and K. W. Schmid, Prog. Part. Nucl. Phys. **5**, 79 (1981).
[31] I. Ragnarsson, T. Bengtsson, W. Nazarewicz, J. Dudek, and G. A. Leander, Phys. Rev. Lett. **54**, 982 (1985).
[32] M. Kortelahti *et al.*, Phys. Lett. **131B**, 305 (1983).
[33] F. A. Beck *et al.*, Phys. Lett. B **192**, 49 (1987).